On The Diffusion of Sticky Particles in 1-D

Joshua DM Hellier* and Graeme J Ackland†
SUPA, School of Physics and Astronomy, University of Edinburgh, Mayfield Road, Edinburgh EH9 3JZ, United Kingdom
(Dated: July 11, 2018)

The 1D Ising model is the simplest Hamiltonian-based model in statistical mechanics. The simplest interacting particle process is the Symmetric Exclusion Process (SEP), a 1D lattice gas of particles that hop symmetrically and cannot overlap. Combining the two gives a model for sticky particle diffusion, SPM, which is described here. SPM dynamics are based on SEP with short-range interaction, allowing flow due to non-equilibrium boundary conditions. We prove that SPM is also a detailed-balance respecting, particle-conserving, Monte Carlo description of the Ising model. Neither the Ising model nor SEP have a phase transition in 1D, but the SPM exhibits a non-equilibrium transition from a diffusing to a blocked state as stickiness increases. We present a fully non-linear, analytic, mean-field solution, which has a crossover from a positive to a negative diffusion constant. Simulations in the positive-diffusion region agree with the analytics. The negative diffusion constant in fact indicates a breakdown of the mean-field approximation, with close to zero flow and breaking into a two-phase mixture, and thus the mean field theory successfully predicts its own demise. The simplicity of the model suggests a wide range of possible applications.

I. INTRODUCTION

Lattice gases are a ubiquitous tool for modeling complex systems from biology to traffic [1–7]. Analytically solvable cases involve non-interacting or excluding particles [8–13], but in any real system of interest the moving objects interact. Many models tackle the situation where the diffusing object interact with the substrate, but despite the clear application-relevance there is surprisingly little work considering interactions between the moving particles themselves. One reason for this is that the interactions introduce nonlinearities in analytical models, which makes them challenging to solve, at least outside of limits in which they can be linearized. This is unfortunate because it is precisely these nonlinearities which introduce interesting behaviors such as discontinuities at the oxide-metal interface or diffusion instability [14, 15].

Another feature of previous models is that the flow is driven by either asymmetry in the dynamics (e.g. ASEP) or an external field which permeates the system (e.g. KLS). In either case, the particles always see a local asymmetry. However in many systems the flow is driven by a pressure or chemical potential difference applied at the boundaries, so that any local asymmetry arises from self-organization. This situation is addressed here.

In this paper we will investigate a simple one-dimensional model, the "Sticky Particle Model" or SPM, specified in the top left inset of Fig. 1, which contains such an interaction, and we will explore the impact this has on particle behavior, in particular when observed in the large-scale limit. One might contrast this approach (making a simple microscopic model and trying to learn from it about large-scale interface growth) with approaches such as the KPZ equation [16–18] (where one analyses the extreme large-scale dynamics using universality classes).

II. THE STICKY PARTICLE MODEL

The SPM is an excluded-particle model in which adjacent particles separate with rate λ and single particles move at rate 1.

It differs from the symmetric exclusion process [19–24]; in that particles "unstick" with rate λ instead of their normal hopping rate, 1. Low λ corresponds to sticky particles, high λ to repelling particles. It could be regarded as a version of the KLS model [25–27] in 1-dimension without an applied field, which is itself similar to the dynamics used to analyze the Ising model by Kawasaki [28]. The KLS model has a field which introduces an asymmetry which drives a flow. It is tacitly assumed that this field is required for the nontrivial flow behavior seen in the model, so the simpler symmetric model has received less attention.

A. Detailed Balance Proof

The SPM is intended to study flow, so it is *defined* by the hopping rates. In Fig. 1 we show all the possible transitions which may occur between local configurations.

Assume that the system is now on a ring, with L lattice sites and N particles. Let us label possible system configurations by ξ and let the number of adjacencies (or "bonds") between particles be $b(\xi)$. Now for our ansatz, assume that the probability of the system being in state ξ is $\lambda^{-b(\xi)}$. In the top and bottom diagrams of Fig. 1 we can see that the number of bonds on both sides is the same, as are the transition rates back and forth; thus our ansatz holds for these states, as it predicts the probabilities of the left and right configurations are the same.

* J.D.M.Hellier@sms.ed.ac.uk
† G.J.Ackland@ed.ac.uk

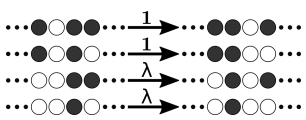

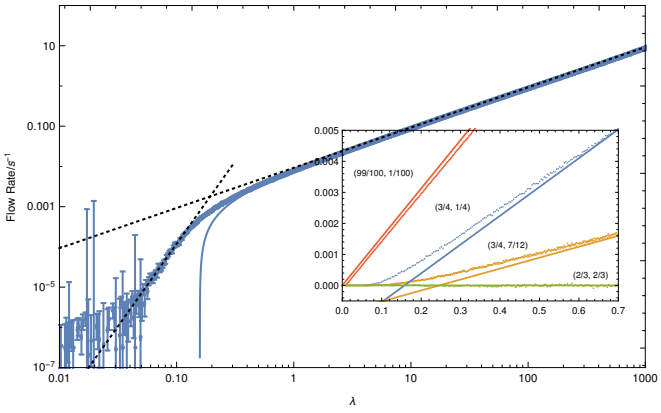

FIG. 1. **Top left:** White circles indicate particles, dark circles indicate empty sites (vacancies). Particles randomly move into adjacent vacancies with rate 1 (having rescaled time for notational convenience), unless there is a particle behind the position they're moving from, in which case they move with rate λ; the state of the site next to the position the particle is moving into is irrelevant. Particles also move to the left, with rates such that the whole model is totally symmetric.
Bottom right: Mean flow rate observed when varying λ with fixed boundary densities (ρ_0, ρ_L) as labeled in the plot. The MFT prediction is indicated by the solid line. In each case we used systems of length 64 (length 32, 128 and 256 give similar results), running them for 4×10^5 Gillespie steps for equilibration followed by 10^4 independent data gathering runs of 10^3 steps, interspersed with relaxation runs of 16000 steps. This way we could gather statistics about flow rates and densities in a well-equilibrated system. Specifically, we generate a pool of 10000 samples of flow rate and density from which we can calculate estimates of the descriptive statistics of both quantities; flow moments and the density data are included in the supplementary materials.
Main figure: As the blue $\left(\frac{3}{4}, \frac{1}{4}\right)$ data on the inset plot, with the same boundary conditions and run parameters, but with both axes logarithmic and over a wide range of orders of magnitude of λ. The dashed lines represent power-laws; the higher-λ one is asymptotically matched to the mean-field prediction, whilst the lower-λ one is fitted to the power-law behavior in the range $0.04 \leq \lambda \leq 0.1$.

The middle two diagrams are equivalent; in the upper diagram a bond is formed going left to right and then broken going right to left, so the probability of being in the left state is λ times that of being in the right state. This is again in agreement with the detailed balance criterion. As these are the only types of transition that may occur on a ring, we have proven that the closed system obeys detailed balance.

B. Equivalence to Ising Model at Equilibrium

Since the model obeys detailed balance, there must be an associated Hamiltonian. This is simply the number of particles stuck together

$$H = \sum_i p_i p_{i+1}$$

where p_i is 1 for a particle or zero for and empty site. A simple transformation $s_i = 2p_i - 1$ shows this to be equivalent to the Ising Hamiltonian

$$H = \sum_i \frac{1}{4} s_i s_{i+1} + \frac{1}{2} s_i + \frac{1}{4}$$

The final term is constant, and only hopping moves are allowed so that $\sum s_i$ is also constant. So at equilibrium the SPM samples the 1D Ising model with fixed magnetisation, a fact which was used to validate the codes.

III. SIMULATIONS

In our system the bulk is perfectly symmetric, and flow is driven by setting ρ at the boundaries, with the system self-organising to give the steady-state density. Thus the boundary concentrations, ρ_0 and ρ_L are the independent variables which drive the system. The flow rate, Hamiltonian energy and particle density of the system are fully determined by (ρ_0, ρ_L) and the unsticking rate λ

We chose to calculate using the `KMCLib`[29] package, which implements the Kinetic Monte Carlo algorithm (essentially the same as the Gillespie algorithm[30–32]) on lattice systems. The codes used are kept here [33].

We are interested in flow in a bounded domain, and can simulate that situation using KMC. In the bulk, the transition rates are simply those described in Fig. 1. At the boundaries there are 2 layers of lattice sites that switch between being full and empty with rates such that the time-averaged occupation (ρ_0, ρ_L) defines the boundary conditions; The system is therefore open, and particles appear and disappear at boundary layers. These boundaries are equivalent to having particle reservoirs attached to the edges of the domain.

Independent of the KMCLib code, we wrote a simple Metropolis-Hastings algorithm which randomly selects single particle hops. Except for extreme λs, this has an acceptance rate of order 10%. Results determined from the KMC and Metropolis-Hastings codes are indistinguishable.

We calculated the flow from the number of particles entering and leaving the system at the boundaries. Since

the model is defined in terms of *rates*, the flow in "particles per unit time" is well defined quantity.

In the simulation, we can vary ρ_0, ρ_L and λ to address three questions: how does λ affect the flow, how does the flowrate depend on the driving force $(\rho_0 - \rho_L)/L$, and how does the density of particles in the system vary.

Using KMClib we studied systems of length 64 (length 32 gives similar results), running them for 400000 Gillispie steps for equilibration followed by 10000 measurement runs of 1000 steps interspersed with relaxation runs of 16000 steps. This way we could gather statistics about flow rates and densities in a well-equilibrated system. Specifically, we generate a pool of 10000 samples of flow rate and density, from which we can calculate estimates of the descriptive statistics of both quantities.

A. Transition in flow character

Fig1 shows how the flowrate varies with stickiness at fixed driving. At high λ the rate is simply proportional to λ for any forcing. This result is far from trivial - it means that the overall flow is determined by the *faster* rate λ, not the slower rate (1). That the MFT averages over the two is unsurprising (Eq. 6), but for the simulation to avoid having a "rate limiting step" requires the system to fill to sufficient density that there are always particles in contact to repel one another.

At low λ the simulation shows a transition to a different behavior, the flow rate remains finite. This transition corresponds to a distinctive peak in the particle density fluctuations $< (\rho - \bar{\rho})^2$ (Fig.2). The width of the peak is independent of the system size which suggests a continuous phase transition from the free flowing to the "stuck" regime.

At very low λ it becomes exceptionally rare for a particle or vacancy to traverse the whole system, the KMC is unable to generate good statistics, and the flow measurement is dominated by the noise of boundary fluctuations. However, there is a regime when $0.04 \leq \lambda \leq 0.1$ where the mean flow again displays clear power-law behavior, this time with $\mathcal{O}\ (\lambda^4)$; between this region and the λ^1 region there is a bend as we switch between the power laws.

B. Effective diffusion constant

Using boundary conditions $(\rho_0, \rho_L) = (\rho_M + \frac{1}{2}\delta\rho, \rho_M - \frac{1}{2}\delta\rho)$ we demonstrate the dependence of flowrate on driving and λ. (Fig 5). This shows that the transition to the stuck phase is suppressed by stronger driving forces (large $|\delta\rho|$)

We use the limit of small $\delta\rho$ to calculate the effective diffusion constant. This is normalised to 1 in the case of $\lambda = 1$, which is just SEP. The $\rho_M = 0$ limit corresponds to free flow of particles, so the diffusion constant here does to 1. Similarly the $\rho_M = 1$ limit is flow of vacancies, so $D \to \lambda$. One might expect a monotonic variation between these limits, but surprisingly the simulations show that there is always an extremal value for D close to $\rho_M = 2/3$: this is a minimum for $\lambda < 1$ and a maximum for $\lambda > 1$

C. Self-organised density

We calculated the time-averaged total number of particles in the system by updating a histogram of particle numbers as the simulation progresses. In each of our calculations, we make the initial configuration by randomly filling the system with particles and vacancies in such a way that the initial density should be $\frac{1}{2}(\rho_0 + \rho_L)$, and then run the system for a sufficient number of equilibration steps to destroy any initial transients.

In SEP, $(\lambda = 1)$ the density varies linearly across the system from ρ_0 to ρ_L, as one expects for a diffusion process. However, for sticky particles, $\lambda < 1$, the density rises sharply near to the boundary, then has a linear profile about a value higher than ρ_M (Fig.4d). One might view this as particles being sucked into the system to lower their Hamiltonian Energy, but such a notion can be dismissed since the internal density *also rises for repelling particles*, $\lambda > 1$. The asymptotic values for the density at high and low σ appear to be 1 and $\frac{2}{3}$, regardless of the mean boundary density ρ_M. Fig 3

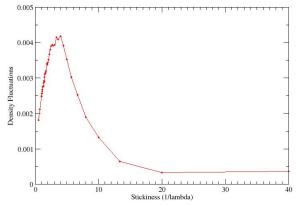

FIG. 2. [Placeholder] Density fluctuation as a function of λ for a range of system sizes with boundary conditions (0.6, 0.4)

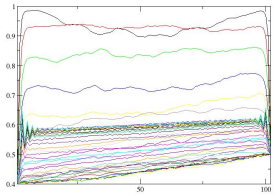

FIG. 3. [Placeholder] Density profile for range of λ from 0-100, with boundary conditions (0.5, 0.4)

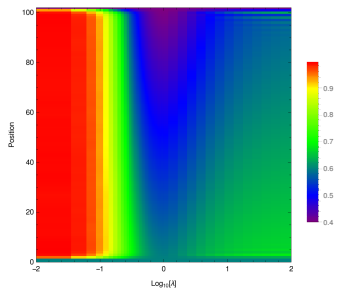

FIG. 4. [Placeholder] Mean density within the flowing system as a function of stickiness for various boundary conditions.

D. Review of the simulations

Simulation of the sticky particle model reveals a number of curious and unexpected features which have no equivalent in either SEP or the 1D Ising model.

- A transition in flow character from λ to λ^4.
- The mean density of the system has complicated variation with λ^4.
- The effective diffusion constant has an extremum value at intermediate boundary density.

To get further understanding of these behaviours, we tackle the system analytically.

IV. MEAN FIELD THEORY FOR FLOW

Let the spacing between lattice sites be a, let τ_0 be the free-particle hopping timescale, and the time-averaged (or ensemble-averaged, assuming ergodicity) occupation probability of the i^{th} lattice site be ρ_i. We will introduce $\zeta = 1 - \lambda$ here for convenience.

1. *Fokker-Planck Equation*

Let the ensemble-averaged occupation probability of the i^{th} site at time t be $\rho_i(t)$. In the mean-field approximation this is assumed to be independent of $\rho_j(t)$ for $j \neq i$ at equal times. Therefore, if the i^{th} site is occupied, then the rate at which it empties is the sum of contributions from the four permutations of the $(i+1)^{\text{th}}$ and $(i-1)^{\text{th}}$ occupancy:

$$\begin{aligned}&\frac{1}{\tau_0}(1-\rho_{i-1})\left[(1-\rho_{i+1})+\lambda\rho_{i+1}\right]\\ +&\frac{1}{\tau_0}(1-\rho_{i+1})\left[(1-\rho_{i-1})+\lambda\rho_{i-1}\right].\end{aligned} \tag{1}$$

Similarly, if the $(i)^{\text{th}}$ site is unoccupied, it fills with rate which depends on the occupation probability of the neighbours, and whether they are stuck to the $(i+2)^{\text{th}}$ and $(i-2)^{\text{th}}$ sites respectively. Therefore, an unoccupied i^{th} site fills with rate

$$\frac{1}{\tau_0}\left\{\rho_{i+1}\left[\lambda\rho_{i+2}+(1-\rho_{i+2})\right]+\rho_{i-1}\left[\lambda\rho_{i-2}+(1-\rho_{i-2})\right]\right\}. \tag{2}$$

If we now multiply the filling/emptying rates of site i by the probablity of being empty/full respectively, we obtain the final Fokker-Planck equation for the site occupaution

$$\begin{aligned}\tau_0\frac{\partial\rho_i}{\partial t} =&(1-\rho_i)\left[(1-\zeta\rho_{i-2})\,\rho_{i-1}+(1-\zeta\rho_{i+2})\,\rho_{i+1}\right]\\ &-\rho_i\left[2\zeta\rho_{i-1}\rho_{i+1}-(3-\zeta)\left(\rho_{i-1}+\rho_{i+1}\right)+2\right].\end{aligned} \tag{3}$$

2. *Diffusion Equation: MFT Continuum Limit*

To obtain the continuum limit of the MFT we substitute $\rho_i(t) \to \rho(x,t)$, $\rho_{i+m}(t) \to \rho(x+am,t)$ into Eq. 3. Then, using a Taylor expansion around x for small a, neglecting terms of $\mathcal{O}(a^4)$, and collecting terms we find that

$$\begin{aligned}\tau_0\frac{\partial\rho}{\partial t} =&a^2\left[1-\zeta\rho(4-3\rho)\right]\frac{\partial^2\rho}{\partial x^2}\\ &+2a^2\zeta(3\rho-2)\left(\frac{\partial\rho}{\partial x}\right)^2+\mathcal{O}(a^4),\end{aligned} \tag{4}$$

which can be factorized into the more familiar form of a continuity equation

$$\frac{\partial\rho}{\partial t}=\frac{a^2}{\tau_0}\frac{\partial}{\partial x}\left\{\left[1-\zeta\rho\left(4-3\rho\right)\right]\frac{\partial\rho}{\partial x}\right\}, \tag{5}$$

having dropped the higher-order terms. From this we can identify the flow $J(x)$ as the term in the curly brackets, and define a mean field diffusion constant (see Fig.6):

$$D_{MFT}(\zeta,\rho)=\frac{a^2}{\tau_0}\left[1-\zeta\rho\left(4-3\rho\right)\right] \tag{6}$$

We note that the MFT diffusion constant can become negative. The density at which this occurs is given by solving Eq.6:

$$\rho_c=\frac{2}{3}\pm\frac{1}{3}\sqrt{(4-3/\zeta)}$$

This has no real solution for $\zeta < 0.75$. So in the limit of very sticky particles ($\lambda < 0.25$) the MFT predicts a transition between forward and backwards diffusion at some densities.

3. Limiting Cases

In order to understand the implications of the MFT, let us consider some limits. As $\zeta \to 0$ (i.e. as the model becomes a simple exclusion model), $D \to \frac{a^2}{\tau_0}$. Likewise, in the dilute limit $\rho \to 0$, $D \to \frac{a^2}{\tau_0}$, reflecting the fact that it becomes a dilute lattice gas and therefore the interactions between particles become irrelevant as they never meet. Conversely, in the full limit $\rho \to 1$, $D \to \frac{\lambda a^2}{\tau_0}$; this is because we now have a dilute gas of vacancies, which hop with rate $\frac{\lambda}{\tau_0}$.

One may observe that the MFT has a symmetry under $\rho \mapsto \frac{4}{3} - \rho$; thus, the dynamics should be symmetric under a density profile reflection around $\rho = \frac{2}{3}$. This is where D always attains its extremal value, $\frac{a^2}{\tau_0}\left[1 - \frac{4}{3}\zeta\right]$, hence for $\zeta > 3/4$ the diffusion coefficient becomes negative in regions with $\frac{2}{3} - \frac{\sqrt{\zeta(4\zeta-3)}}{3\zeta} < \rho < \frac{2}{3} + \frac{\sqrt{\zeta(4\zeta-3)}}{3\zeta}$.

Finally, it is possible to show that solutions to the continuum MFT containing domains with a negative diffusion coefficient are linearly unstable; thus, if we try to have a flow containing ρ for which $D(\rho) < 0$, the density of the medium should gravitate towards one of the two densities for which $D(\rho) \sim 0$. Instead of observing "backwards diffusion" we would see an extremely slow flow or no flow at all.

4. Steady State Flow

It is possible to solve the continuum MFT in a steady state on a finite domain, say $x \in (0, L)$. Steady state implies that there is no build-up of particles $\frac{\partial \rho}{\partial t} = 0$, so the flow is constant through the system.

Using the constant-flow requirement for continuity $J(x) = J_0 = \text{const.}$, and by integrating both sides of equation5 with respect to x we find that:

$$\int_{x_0}^{x} J(x')dx' = -\frac{a^2}{\tau_0}\int \mathrm{d}\rho\left[1 - \zeta\rho\left(4 - 3\rho\right)\right] \tag{7}$$

$$(x - x_0)J_0 = -\frac{a^2}{\tau_0}\left[\rho + \zeta(\rho - 2)\rho^2\right] \tag{8}$$

The density profile across the system is given by solving for $\rho(x)$. Since Eq.8 is cubic, the solution for density $\rho(x)$ is non-unique for cases of high ζ. Thus in the limit of high stickiness, the MFT is unable to make a unique prediction for the density. Furthermore, except in the SEP case $\zeta = 0$, the density will not vary linearly across the system.

5. Dirichlet Boundary Conditions

The constants x_0 and J_0 are the boundary conditions for the flow, but they need not correspond to a physically-realisable situation. For driven systems it is more convenient to consider fixing the density at each end.

If we impose such Dirichlet boundary conditions on this system, say $\rho(0) = \rho_0$ and $\rho(L) = \rho_L$, we find that

$$J_0 = \frac{a^2}{L\tau_0}\left[\rho_0 - \rho_L + \zeta\left(\rho_0\left[\rho_0^2 - 2\right] - \rho_L\left[\rho_L^2 - 2\right]\right)\right]. \tag{9}$$

This equation can be used for direct comparison with the simulations (Figs.5,6. In general, the agreement is good, except for the region where the MFT predicts negative flow.

6. Interpretation of MFT

The mean field theory enables us to predict flow behaviour of the MFT. It recovers well-known limiting cases such as SEP ($\lambda = 0$), however at high stickiness ($\lambda < 0.25$) it predicts its own demise, with unphysical negative diffusion constants and by having multiple solutions for the density at some positions in the system. Moreover, at these conditions, the MFT does not give a unique density profile. This breakdown of the MFT corresponds to the transition to slow flow observed in the simulation.

In some conditions MFT predicts densities greater than 1. One might guess that when the MFT offers two possible values for the density, it will correspond to a phase separation transformation in the actual system. Furthermore, the MFT prediction of a maximum diffusion constant at a density of $\rho = 2/3$ suggests that this value of ρ might be favoured for strongly driven flows.

A curious feature of the MFT diffusion (Fig. 6) is that for fixed stickiness there are *two possible densities* giving the same diffusion constant. Thus it is possible to have a steady state flow with phase separation into regions of high and low density. This echoes the situation seen in short time-averages of the simulation (Fig.7) where blocks of high and low density are evident.

Regarding the phase transition, we should note that we only have an MFT prediction for the flow rate as a function of λ, since $\rho(x)$ stops being unique when λ drops below $\frac{1}{4}$, and so the MFT lacks predictive power. For low-stickiness, when $\lambda > \frac{1}{4}$, the MFT is in very good agreement with the simulations, and this continues as λ stretches into the thousands, where the mean flow varies as $\mathcal{O}(\lambda^1)$.

The MFT prediction for the mean flow is again a good fit until λ becomes sufficiently small, and as before the simulations show no evidence of negative diffusion; rather the flow becomes critically slow for very sticky particles. The higher moments of the flow (e.g. variance) do not show peaks, indicating that hard transitions are not occurring. Finally, the density is very close to the average of the boundary densities until λ drops below 1/4, at which point the system fills.

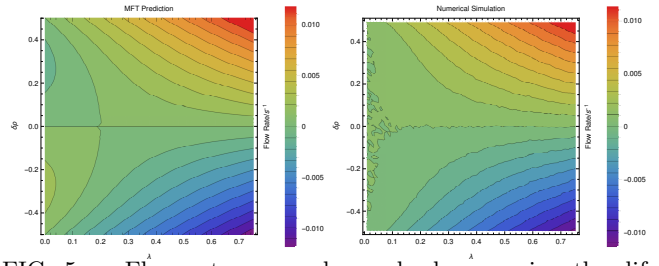

FIG. 5. Flow rate mean observed when varying the difference $\delta\rho$ between the boundary concentrations $(\rho_0, \rho_L) = (\rho_M + \frac{1}{2}\delta\rho, \rho_M - \frac{1}{2}\delta\rho)$ and λ (The top panel is the MFT prediction for the flow rate, whilst bottom shows the observed mean flow rate). We chose $\rho_M = \frac{1}{2}$, as this gives us the biggest range of $\delta\rho$ to investigate. These calculations were performed with the same run parameters (system length etc) as above. The MFT prediction (Fig.5a) shows a region of negative flow - this occurs at $\zeta > \frac{4}{5}$ for the weakest driving force, with additional stickiness required when the driving force increases. The simulation exhibits close to zero flow in that region (Fig.5b). Away from this region, the MFT and the simulation are in good agreement.

Continuing to specify the boundary densities to be $(\rho_0, \rho_L) = (\rho_M + \frac{1}{2}\delta\rho, \rho_M - \frac{1}{2}\delta\rho)$ for some given ρ_M, we can keep $\delta\rho$ relatively small, so that J varies approximately linearly with $\delta\rho$; thus if we calculate J for a series of small $\delta\rho$, we can perform linear regression to find $D_{\text{Eff}} = \frac{\partial J}{\partial \delta\rho}\Big|_{\delta\rho=0}$, the effective diffusion coefficient. Computing this for different (ρ_M, λ) combinations yields results that can be compared with Eq. 9.

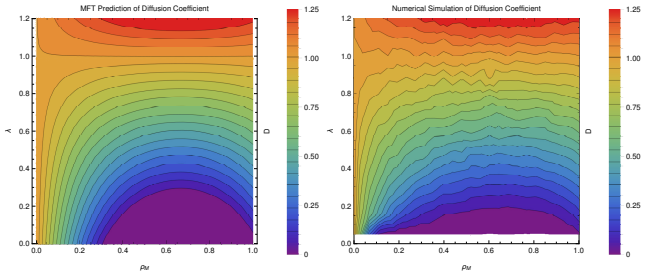

FIG. 6. Comparison of effective diffusion coefficient D in the MFT (top) and in direct simulation (bottom) as a function of density and stickiness. The white region is where the MFT gives negative diffusion. The simulations used 124 sites averaged over $\sim 10^9$ steps at each of $12 \times 24 \times 16$ $(\lambda, \rho_M, \delta\rho)$ combinations. Full details in the supplementary materials.

We compare the MFT prediction and the actual numerical results for the diffusion constant in Fig. 6. We see that MFT and simulation agree well for low stickiness, and both show the symmetry about $\rho_M = \frac{2}{3}$. For high stickiness, where the MFT prediction gives negative diffusion constant, we once again see low positive values for the current. It should be noted that the MFT assumes that $\rho = \rho_M$ throughout, whereas in the simulations ρ tends to be much higher.

It is instructive to get an overview of how the particles move during flow. Fig. 7 show a plot of the flow structure in the slow-flow regime. In very short time averages the "striped" pattern indicates separation into dense and sparse regions, with an overall concentration gradient arising from the relative size of such regions. Particle/vacancy diffusion through the empty/full regions can be seen. As the averages are taken over longer times the blocks themselves appear to diffuse. Averaged over the entire simulation (not shown) the averaging simply gives a smooth density gradient.

Interesting structure is visible, the dynamics appearing as a random walk with some tendency for particles to clump; over longer timescales the diffusive behavior is more evident, with a textured structure suggesting characteristic velocity of particles or vacancies through emergent correlated clumps. Additional plots can be found in the supplementary materials.

FIG. 7. Indicative spacetime flow pattern for sticky free-flow $\left[\lambda = \frac{3}{20}, (\rho_0, \rho_L) = (\frac{3}{4}, \frac{1}{4})\right]$; other combinations shown in the supplementary materials. Time runs along the x-axis, space (1 pixel=1 site) along the y-axis, with grayscale tone (black being empty, white being full) illustrating average site occupation over (clockwise from top left) $\frac{1}{32}$, 1, 8 and 32 Gillespie steps per site respectively.

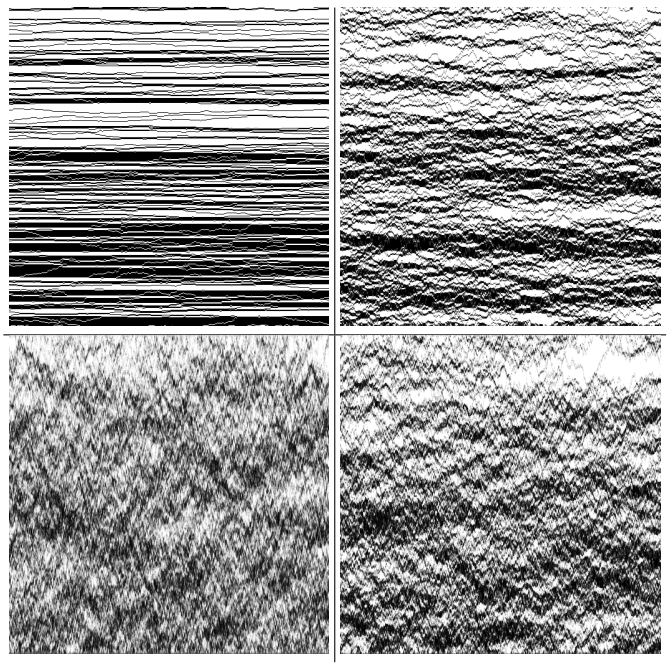

V. DISCUSSION AND CONCLUSIONS

The sticky particle model is the combination of the Ising model with symmetric exclusion process. It arguably represents the simplest possible flow model for interacting particles is a homogeneous medium.

Although only the particles exhibit stickiness, the analytics suggest a symmetry between vacancy-type and

particle-type flow at density of $\frac{2}{3}$, which is observed in the simulation. The flow exhibits a foamy pattern with intermediate time-and-space correlations. The continuum solution MFT is a good predictor of the bulk flow behavior of the SPM. The negative diffusion constant found in MFT at high stickiness indicates that the assumption of homogeneous density break down: thus the MFT predicts its own demise, and this agrees well with our numerics.

Above a certain level of stickiness, the model exhibits a nonequilibrium phase transition to a slow-flowing phase. The require stickiness for the transition is dependent on the strength of the driving force - a strongly driven system inhibits the flow. Mean field analysis, together with visualization of the flowing system, suggest that the transition comes when the density becomes inhomogeneous.

A number of questions remain open. Is there a physical principle which determines the density? Why does the strongly repelling system produce a density with maximum flow? Can one derive the λ^4 dependence of the slow-flow?

ACKNOWLEDGEMENTS

We would like to thank EPSRC (student grant 1527137) and Wolfson Foundation and ERC for providing funding, Mikael Leetmaa for producing `KMCLib`, and the `Eddie3` team here at Edinburgh for maintaining the hardware used. We would also like to thank Martin Evans, Bartek Waclaw and Richard Blythe for some very helpful discussions.

[1] V. Belitsky and G. M. Schütz, Journal of Statistical Mechanics: Theory and Experiment **2011**, P07007 (2011).
[2] M. Mobilia, I. T. Georgiev, and U. C. Täuber, Journal of Statistical Physics **128**, 447 (2007).
[3] B. Tegner, L. Zhu, C. Siemers, K. Saksl, and G. Ackland, Journal of alloys and compounds **643**, 100 (2015).
[4] L. Zhu, Q.-M. Hu, R. Yang, and G. Ackland, Journal of Physical Chemistry C **116**, 24201 (2012).
[5] B. E. Deal and A. S. Grove, Journal of Applied Physics **36**, 3770 (1965), https://doi.org/10.1063/1.1713945.
[6] N. Cabrera and N. F. Mott, Reports on Progress in Physics **12**, 163 (1949).
[7] S. Buzzaccaro, R. Rusconi, and R. Piazza, Phys. Rev. Lett. **99**, 098301 (2007).
[8] A. J. C. Ladd, M. E. Colvin, and D. Frenkel, Phys. Rev. Lett. **60**, 975 (1988).
[9] T. M. Liggett, *Interacting particle systems* (Springer-Verlag, Berlin, 1985).
[10] E. Ben-Naim, S. Y. Chen, G. D. Doolen, and S. Redner, Phys. Rev. Lett. **83**, 4069 (1999).
[11] S. F. Shandarin and Y. B. Zeldovich, Rev. Mod. Phys. **61**, 185 (1989).
[12] L. Frachebourg, Phys. Rev. Lett. **82**, 1502 (1999).
[13] L. Frachebourg, P. A. Martin, and J. Piasecki, Physica A Statistical Mechanics and its Applications **279**, 69 (2000), cond-mat/9911346.
[14] V. V. Obukhovsky, A. M. Kutsyk, V. V. Nikonova, and O. O. Ilchenko, Phys. Rev. E **95**, 022133 (2017).
[15] N. V. Gorokhova and O. E. Melnik, Fluid Dynamics **45**, 679 (2010).
[16] M. Kardar, G. Parisi, and Y.-C. Zhang, Phys. Rev. Lett. **56**, 889 (1986).
[17] J. Krug and H. Spohn, Phys. Rev. A **38**, 4271 (1988).
[18] T. Sasamoto and H. Spohn, Phys. Rev. Lett. **104**, 230602 (2010).
[19] K. E. P. Sugden and M. R. Evans, Journal of Statistical Mechanics: Theory and Experiment **2007**, P11013 (2007).
[20] M. Kollmann, Phys. Rev. Lett. **90**, 180602 (2003).
[21] B. Lin, M. Meron, B. Cui, S. A. Rice, and H. Diamant, Phys. Rev. Lett. **94**, 216001 (2005).
[22] C. Hegde, S. Sabhapandit, and A. Dhar, Phys. Rev. Lett. **113**, 120601 (2014).
[23] P. L. Krapivsky, K. Mallick, and T. Sadhu, Phys. Rev. Lett. **113**, 078101 (2014).
[24] T. Imamura, K. Mallick, and T. Sasamoto, Phys. Rev. Lett. **118**, 160601 (2017).
[25] S. Katz, J. L. Lebowitz, and H. Spohn, Journal of Statistical Physics **34**, 497 (1984).
[26] R. K. P. Zia, Journal of Statistical Physics **138**, 20 (2010).
[27] Y. Kafri, E. Levine, D. Mukamel, G. M. Schütz, and R. D. Willmann, Phys. Rev. E **68**, 035101 (2003).
[28] K. Kawasaki, Phys. Rev. **145**, 224 (1966).
[29] M. Leetmaa and N. V. Skorodumova, Computer Physics Communications **185**, 2340 (2014), arXiv:1405.1221 [physics.comp-ph].
[30] D. T. Gillespie, The Journal of Physical Chemistry **81**, 2340 (1977), http://dx.doi.org/10.1021/j100540a008.
[31] A. Bortz, M. Kalos, and J. Lebowitz, Journal of Computational Physics **17**, 10 (1975).
[32] A. Prados, J. J. Brey, and B. Sánchez-Rey, Journal of Statistical Physics **89**, 709 (1997).
[33] J. Hellier, (2018), 10.5281/zenodo.1162818.